ACS NANO

www.acsnano.org

ARTICLE

Complex Stoichiometry-Dependent Reordering of 3,4,9,10-Perylenetetracarboxylic Dianhydride on Ag(111) upon K Intercalation

Christian Zwick,[†] Anu Baby,[‡,§] Marco Gruenewald,[†] Elisabeth Verwüster,[‡] Oliver T. Hofmann,[‡] Roman Forker,[†] Guido Fratesi,[⊥,§] Gian Paolo Brivio,[§] Egbert Zojer,[‡] and Torsten Fritz*[,†,∥]

[†]Institute of Solid State Physics, Friedrich Schiller University Jena, Helmholtzweg 5, 07743 Jena, Germany

[‡]Institute of Solid State Physics, NAWI Graz, Graz University of Technology, Petersgasse 16, 8010 Graz, Austria

[§]Department of Materials Science, University of Milano-Bicocca, Via R. Cozzi 55, 20125 Milano, Italy

[⊥]Dipartimento di Fisica, Università degli Studi di Milano, Via Celoria 16, 20133 Milano, Italy

[∥]Graduate School of Science and Institute for Academic Initiatives, Department of Chemistry, Osaka University, 1-1 Machikaneyama, Toyonaka 560-0043, Osaka, Japan

Supporting Information

ABSTRACT: **Alkali metal atoms are frequently used for simple yet efficient n-type doping of organic semiconductors and as an ingredient of the recently discovered polycyclic aromatic hydrocarbon superconductors. However, the incorporation of dopants from the gas phase into molecular crystal structures needs to be controlled and well understood in order to optimize the electronic properties (charge carrier density and mobility) of the target material. Here, we report that potassium intercalation into the pristine 3,4,9,10-perylenetetracarboxylic dianhydride (PTCDA) monolayer domains on a Ag(111) substrate induces distinct stoichiometry-dependent structural reordering processes, resulting in highly ordered and large K_xPTCDA domains. The emerging structures are analyzed by low-temperature scanning tunneling microscopy, scanning tunneling hydrogen microscopy (ST[H]M), and low-energy electron diffraction as a function of the stoichiometry. The analysis of the measurements is corroborated by density functional theory calculations. These turn out to be essential for a correct interpretation of the experimental ST[H]M data. The epitaxy types for all intercalated stages are determined as point-on-line. The K atoms adsorb in the vicinity of the oxygen atoms of the PTCDA molecules, and their positions are determined with sub-Ångström precision. This is a crucial prerequisite for the prospective assessment of the electronic properties of such composite films, as they depend rather sensitively on the mutual alignment between donor atoms and acceptor molecules. Our results demonstrate that only the combination of experimental and theoretical approaches allows for an unambiguous explanation of the pronounced reordering of K_xPTCDA/Ag(111) upon changing the K content.**

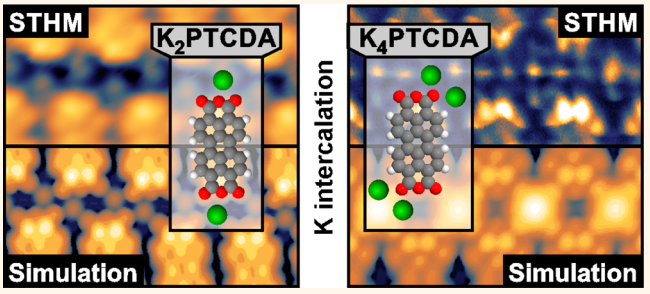

KEYWORDS: *potassium intercalation, self-assembled nanostructures, low-temperature scanning tunneling microscopy (LT-STM), scanning tunneling hydrogen microscopy (STHM), density functional theory (DFT), low-energy electron diffraction (LEED)*

Technologically relevant electric conductivities σ can be achieved through doping, which has become a vital concept for efficient device architectures.[1,2] Alkali metals are frequently employed as electron donors due to their comparatively small ionization energies and relatively straightforward processability.[3−6] Molar doping ratios x (*i.e.*, number of dopants per host molecule) on the order of several percent already lead to a substantial increase of σ.[4] Higher ratios x have been shown to boost σ by as much as 6 orders of magnitude, as demonstrated for the prototypical dye molecule 3,4,9,10-perylenetetracarboxylic dianhydride (PTCDA, $C_{24}H_8O_6$, CAS registry no. 128-69-8) intercalated with potassium.[3] Since then, the interaction of PTCDA with alkali metal atoms has attracted considerable attention, particularly with regard to electronic and optical properties.[7−14]

The microscopic molecular structures formed during doping, although crucial for the understanding of the associated physical properties, are not yet well established. Predominantly

Received: November 12, 2015
Accepted: December 30, 2015
Published: December 30, 2015

DOI: 10.1021/acsnano.5b07145
ACS Nano 2016, 10, 2365−2374

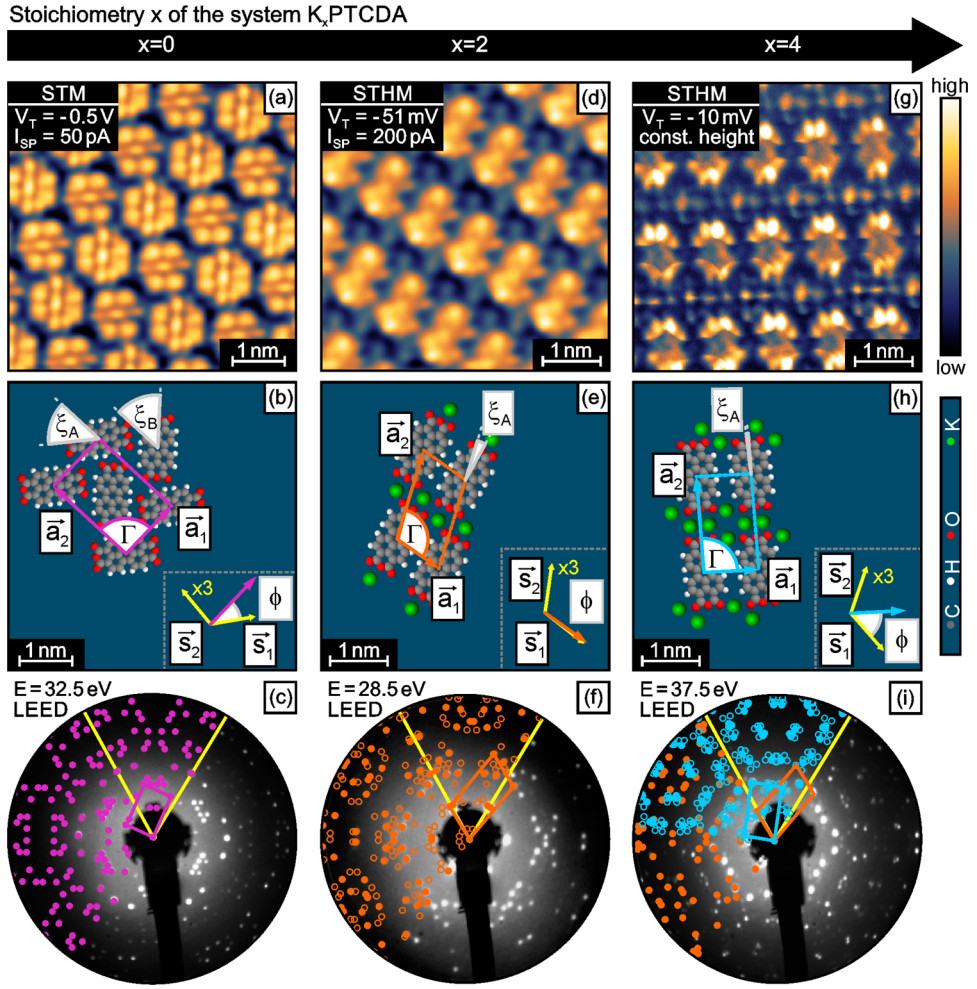

Figure 1. Self-assembled structures of distinct K$_x$PTCDA phases on Ag(111) for x = 0, 2, and 4. (a), (b), and (c) show the STM image, structural model, and LEED image of pristine PTCDA/Ag(111). STHM images associated with x = 2 (d) and x = 4 (g) exhibit features originating from both K and PTCDA. Note that the determination of the unit cell compositions, especially for x = 4, is not straightforward and relies on the comparison with DFT calculations, discussed in the text. The deduced structural models are depicted for x = 2 (e) and x = 4 (h). In each LEED image (c), (f), and (i), the simulated reciprocal unit cell of the associated K$_x$PTCDA structure (x = 0 purple, x = 2 orange, and x = 4 blue) and the silver surface orientation along (01) and (10) (yellow) are superimposed. All possible rotational and mirror domains are considered for the simulation, and when taking multiple scattering into account (open circles), all visible spots are consistent with the model and none remain unidentified. The LEED image shown in (i) belongs to a substrate area simultaneously exhibiting domains corresponding to x = 2 and x = 4. Displayed quantities: V_T bias voltage; I_{SP} tunneling current; E beam energy; $\vec{a}_1$, $\vec{a}_2$ adsorbate lattice vectors; $\Gamma = \angle(\vec{a}_1,\vec{a}_2)$ adsorbate unit cell angle; $\vec{s}_1$, $\vec{s}_2$ substrate lattice vectors with unit cell angle of $\angle(\vec{s}_1,\vec{s}_2) = 120°$; $\phi = \angle(\vec{s}_1,\vec{a}_1)$ domain angle; $\xi_{(A/B)} = (\vec{a}_2,\vec{m}_{(A/B)})$ orientation of molecules A and B in the unit cell.

van der Waals bound molecular crystals are prone to reordering processes upon intercalation with atoms leading to new crystalline or amorphous phases.[15−21] For doped molecular thin films in the monolayer regime the presence of an interface with the substrate further increases the complexity of the system by providing additional interaction channels and, thus, possibly influencing the physical and electronic structures extensively. The intercalation-induced modification of lattice parameters of thin molecular films can be observed, *e.g.*, with low-energy electron diffraction (LEED) and scanning tunneling microscopy (STM). However, the precise experimental determination of the dopant *sites* is rather challenging owing to the usually blurred electronic contrast obtained in STM for adsorbates on metal surfaces.[19,20]

As a promising strategy to tackle this drawback, scanning tunneling hydrogen microscopy (STHM) introduced by Temirov *et al.* may be used.[22] The application of this technique goes well beyond STM by allowing small amounts of hydrogen between the tunneling tip and the sample and subsequently driving the tip−sample distance into the Pauli repulsive regime. Depending on the scanning parameters one can attain a submolecular topographic contrast reminiscent of the corresponding skeletal formula of the compound.[22,23] Nevertheless, with STHM a direct imaging of guest atoms in a molecular host matrix is quite challenging and has not yet been achieved, supposedly because imaging of the molecular and atomic orbitals often requires different tunneling parameters. So far, intercalated atoms were inferred only indirectly from the visualization of bonding channels between molecule and dopant.[24]

In this paper, we adapt the STHM technique to image simultaneously PTCDA molecules and potassium atoms for K$_x$PTCDA complexes of varying stoichiometries in monolayer domains on a Ag(111) surface. This is realized by tuning the tunneling conditions such that the recorded signal is close enough to the ideal STHM case for highly resolved

DOI: 10.1021/acsnano.5b07145
ACS Nano 2016, 10, 2365−2374

Table 1. Structural Data of the Distinct K_xPTCDA Phases on Ag(111) Using the Same Nomenclature as in Figure 1[a]

x	$\lvert\vec{a}_1\rvert$ (Å)	$\lvert\vec{a}_2\rvert$ (Å)	Γ (deg)	A_{PTCDA} (Å^2)	$\xi_{(A/B)}$ (deg)	ϕ (deg)	epitaxy matrix M
0	12.59(1)	18.95(2)	90.99(5)	119.3(2)	+49(3) −50(3)	36.60(4)	$\begin{bmatrix} 5.00(1) & 3.00(1) \\ -1.00(1) & -6.00(1) \end{bmatrix}$
2	8.92(1)	16.05(2)	108.60(9)	135.7(4)	−12(4)	2.63(8)	$\begin{bmatrix} 3.16(1) & 0.16(1) \\ 0.98(1) & 5.98(1) \end{bmatrix}$
4	9.57(1)	16.77(2)	91.66(1)	160.4(4)	+2(3)	51.68(6)	$\begin{bmatrix} 3.55(1) & 3.00(1) \\ -2.65(1) & 4.00(1) \end{bmatrix}$

[a]All unit cell parameters are derived from LEED measurements, except the molecular orientations $\xi_{(A/B)}$ determined from ST[H]M measurements. The average area per molecule A_{PTCDA} is the unit cell area divided by the number of molecules per unit cell. Experimental uncertainties of the last significant digit are given in parentheses.

submolecular contrast of PTCDA but still contains a sufficient contribution of the local electron density of states to identify the K atoms as well. This then enables a detailed observation of the unit cell composition. By controlling the amount of intercalated potassium, distinct highly ordered and large domains of K_2PTCDA and K_4PTCDA complexes can be prepared. The epitaxial relations of both intercalation concentrations are classified as point-on-line (POL) with respect to the silver substrate, substantiated by means of distortion-corrected quantitative LEED measurements. However, especially for the K_4PTCDA phase the ST[H]M images exhibit an ambiguous feature which can only be understood correctly in combination with density functional theory (DFT) calculations. With this interplay between the complementary information acquired from LEED, ST[H]M, and DFT, we gain comprehensive insight into the formed structures, which is indispensable for future evaluations of the electronic properties of alkali-metal intercalated interfaces.

RESULTS AND DISCUSSION

First K Intercalation Stage: K_2PTCDA. As a starting point for the structural investigations we prepared a pristine PTCDA film on Ag(111), ca. 0.7 MLE (monolayer equivalent) thick, which consists of highly ordered, densely packed molecular domains exhibiting the well-known herringbone motif shown in Figure 1a,b.[25−28] Part of the silver surface is deliberately left uncovered to allow for possible structural rearrangements without forcing molecules to adopt adsorption sites in the second layer. By depositing potassium onto these monolayer domains of PTCDA/Ag(111), the herringbone structure is converted into a new highly ordered self-organized phase, hereafter named K_2PTCDA according to the stoichiometry whose determination is described in the following. Large domains of K_2PTCDA complexes exhibiting a rather low defect density can be observed. Moreover, almost no molecules were found in the former herringbone structure or in a disordered phase even without annealing the sample. Hence, the structural transition from the pristine PTCDA herringbone structure to a new highly ordered structure is spontaneous and affects practically all molecular domains.

By means of LEED (Figure 1f), we find a unit cell with significantly shorter lattice vectors ($\lvert\vec{a}_1\rvert$ and $\lvert\vec{a}_2\rvert$ decrease by 29.9% and 15.4%, respectively) and an increased unit cell angle Γ as compared to the initial commensurate herringbone structure (cf. Table 1). Further, the epitaxial relation is a point-on-line (POL) coincidence, as can be inferred from the differences between the epitaxy matrix elements in each row being integer numbers. This is equivalent to a column of integer elements in the epitaxy matrix, provided that $\angle(\vec{s}_1,\vec{s}_2) = 120°$ (as chosen here for the Ag(111) surface).[29]

In order to obtain deeper insight into the unit cell composition, we acquired STHM images which simultaneously feature submolecular resolution of PTCDA as well as clearly resolved potassium atoms. This is hardly achievable in conventional STM mode (cf. Figure 1d and Figure 2a,c). Various samples and STHM conditions were studied to avoid possible misinterpretations. According to these tests, we can rule out experimental artifacts, such as features caused by double tips.

The STHM image in Figure 1d reveals that the adsorbate unit cell of the K_2PTCDA phase consists of only one PTCDA molecule and two potassium atoms. Although the total unit-cell area decreases (*vide supra*), the net area per PTCDA molecule increases by 13.7% as there is only one molecule per K_2PTCDA surface unit cell compared to two molecules for the herringbone arrangement of the pristine PTCDA layer. The STHM image further shows that potassium is incorporated in-plane into the molecular film close to the short edge of PTCDA. Upon closer inspection, the potassium atoms are located near the oxygen atoms and exhibit rather similar bonding distances to PTCDA as compared to the calculated structure of free-standing K_2PTCDA complexes.[10] It has been shown that such a structure is a consequence of an ionic bonding between the alkali metal and PTCDA resulting in PTCDA dianion formation.[8,11]

By inspecting domains of the K_2PTCDA phase (cf. Figure 1d) with STHM, the formed complex shows a characteristic stripelike assembly of alternating rows of PTCDA and K, both oriented along the short lattice vector $\vec{a}_1$, with the molecules oriented nearly perpendicular to the stripe axis. The relative shift of molecules in adjacent rows of PTCDA offers the densest packing and a coordination maximum of the intercalated potassium toward the carboxylic groups. One can view the situation as one-dimensional PTCDA stripes between which rows of K atoms are intercalated (*i.e.*, a reduced dimensionality analogous to conventional intercalation of atoms between 2D extended layers).[30] It is noteworthy that the Ag(111) surface remains structurally unaltered upon K deposition. This is fundamentally different from the situation encountered for the Ag(110) surface, which was previously found to reconstruct significantly when K is evaporated onto a predeposited PTCDA monolayer with subsequent annealing.[18] There the smaller packing density of the Ag(110) surface (whose atoms retain a lower coordination number) allows for

DOI: 10.1021/acsnano.5b07145
ACS Nano 2016, 10, 2365−2374

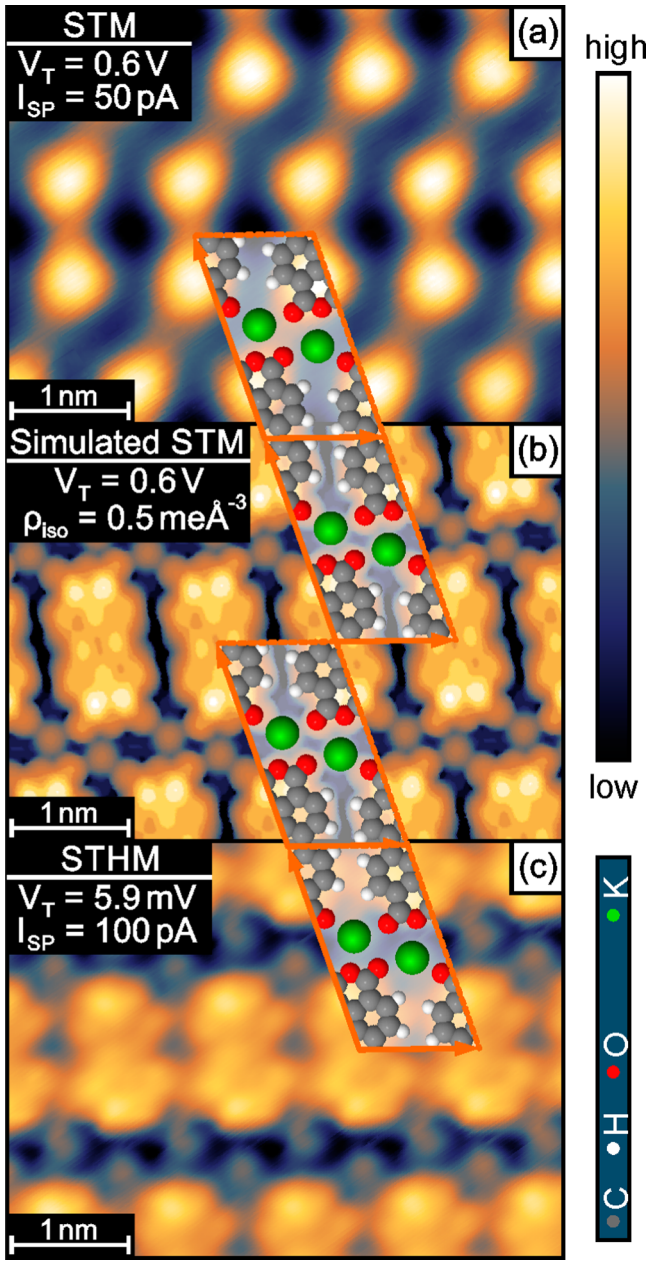

Figure 2. Comparison of experimental STM and STHM images (a, c) with a simulated STM image (b) of the K_2PTCDA phase. The main features originate from the PTCDA molecules, while the K atoms cause small single dots in STHM only. Note that in conventional STM (a) the features are smeared out; PTCDA and K cannot be distinguished. The adsorbate unit cell (orange boxes) comprising the structural model is superimposed in a semi-transparent manner. The applied tunneling parameters V_T (bias voltage), I_{SP} (tunneling current), and ρ_{iso} (isovalue of the integrated density of states) are indicated.

an incorporation of K into the topmost silver layer, resulting in a long-range "potassium-induced missing row reconstruction".[18] Since our experiments were performed without post-growth annealing and revealed no surface reconstruction it is unlikely that K diffused into the topmost densely packed Ag(111) atomic layer. Instead, it was exclusively found intercalated in between PTCDA molecules, *i.e.*, neither underneath nor on top of the molecular layer.

To further substantiate the proposed structural model for the K_2PTCDA phase on Ag(111), the experimentally determined unit cell and stoichiometry were used for DFT calculations. The geometry of PTCDA and K within the unit cell was allowed to structurally relax. Given that the epitaxy type of K_2PTCDA is not commensurate but point-on-line with respect to Ag(111), the silver unit cell had to be slightly modified in order to achieve a geometry consistent with periodic boundary conditions (*i.e.*, a fully commensurate arrangement), necessary for the calculations. In principle, a quasi-commensurate structure with an all-integer epitaxy matrix could also have been achieved by slightly modifying the unit cell of the adsorbate, but we intentionally kept the experimentally determined dimensions in order not to modify the distances between the K atoms and PTCDA molecules. This is done bearing in mind the crucial role played by the interactions between the K atoms and the carboxylic and anhydride oxygen atoms. The necessary changes in the Ag surface lattice constants were small (between 1.0% and 2.6%), and we ensured that the resulting changes in the relaxation of the interlayer spacing (on the order of 0.03 Å) and metal work-function (smaller than 0.04 eV) were negligible. For more details, see the Methods section and the Supporting Information.

Based on the optimized structure, we simulated STM images using the Tersoff–Hamann approach.[31] This provides a first approximation of STM images assuming an s-type tip wave function, an aspect critically assessed in the Supporting Information. Based on the considerations presented there and bearing in mind that for the tunneling conditions used here the STHM images comprise sufficient contributions of the local electron density of states (*vide supra*), a comparison of the Tersoff–Hamann results with these images appears justified, although for a full quantitative understanding of STHM higher angular momentum contributions (for example p-type wave functions) can become relevant as well.[32]

Indeed, when comparing the simulation in Figure 2b with the experimental ST[H]M images in Figure 2a,c, distinct similarities can be found. While the experimentally determined basis is clearly reproduced by the calculations, the features corresponding to PTCDA and K need to be discussed further: The simulated STM image reveals that the strongest features stem from the C–C bonds near the PTCDA anhydride groups. This might also be inferred from the experimental STM image in Figure 2a; however, the experimental features are strongly broadened and, consequently, the potassium atoms remain unresolved. In contrast, most of the intramolecular details from the calculation are clearly visible in the STHM image in Figure 2c, which supports the general assignment of the surface unit cell. We observe distinct spotlike features stemming from the in-plane incorporated potassium as well as features arising from PTCDA. In comparable STHM experiments on a $K_{0.5}$PTCDA phase on Au(111) the K atoms were not resolved directly.[24] The experimentally characterized K_2PTCDA structure (shown in Figure 1e) fully agrees with the geometry-optimized structure obtained from DFT, cf. Figure 2b. This also implies that most likely no further potassium is situated underneath or on top of the PTCDA layer. Furthermore, the DFT analysis shows that upon K intercalation the oxygens of the functional groups of PTCDA tend to bend away from the surface (see Supporting Information), an effect that has been observed experimentally for K intercalated PTCDA on Ag(110) in a similar way.[18] This is in stark contrast to the situation on

DOI: 10.1021/acsnano.5b07145
ACS Nano 2016, 10, 2365–2374

Ag(111) in the absence of K intercalation where the carboxylic oxygens are bent toward the silver surface.[33] In passing, we note that the STHM contrast can be tuned to improve the submolecular resolution of PTCDA even further, however, at the expense of the visibility of K atoms in the same scan (more details, including STHM images for various tunneling parameters, are included in the Supporting Information).

Another interesting outcome of the simulations concerns the layer formation energy of the K_2PTCDA monolayer. It is defined as the energy difference between the bound monolayer and the sum of the contributions from the free metal surface and from the individual constituents of the adsorbate layer (for a strict definition of the quantity see the Methods). The binding energy per molecule for the K_2PTCDA phase is 11.61 eV, which is significantly larger than for phases of PTCDA in the well-known herringbone structure (4.01 eV per molecule) and for the K atoms far apart from each other (2.49 eV per K atom), pointing to an energy gain due to the intercalation, which amounts to 2.62 eV per PTCDA molecule. Such a strong bonding between K atoms and PTCDA molecules in the monolayer is consistent with the efficient formation of the ordered K_2PTCDA phase even without annealing, as discussed above.

Second K Intercalation Stage: K_4PTCDA. By further controlled evaporation of K, the former K_2PTCDA phase is converted into a second highly ordered intercalation stage whose stoichiometry is unraveled only as an outcome of the combined experimental and theoretical efforts detailed below. In anticipation of the results and in order to avoid ambiguity in the terminology used, this phase will be referred to as K_4PTCDA. The transition from K_2PTCDA to K_4PTCDA occurs directly, as evidenced by our LEED investigations, which reveal no intermediate structure. The corresponding STHM and LEED images are shown in panels g and i of Figure 1. By means of ST[H]M, large domains of the K_4PTCDA complexes are observed. They generally also exhibit a low defect density, but their structural perfection is slightly inferior to the K_2PTCDA phase; *i.e.*, the average domain size is smaller and the number of defects appears somewhat increased.

The LEED analysis reveals a significant change of the lattice parameters compared to the former K_2PTCDA phase. Both unit cell vectors increase in length ($|\vec{a}_1|$ and $|\vec{a}_2|$ increase by 7.3% and 4.6%, respectively), while their enclosed angle Γ decreases (cf. Table 1). The epitaxy matrix contains one column of integer numbers; thus, a point-on-line coincidence can be stated also in this case.[29] Note that in LEED experiments with average molar ratios x between 2 and 4, coexisting K_2PTCDA and K_4PTCDA phases were often found on the same sample (cf. Figure 1i), indicating that on macroscopic scales the layer is not necessarily uniform. Notably, the relative intensity of the LEED spots associated with K_4PTCDA could be successfully increased at the expense of those associated with the K_2PTCDA phase by additional potassium deposition.

In addition to conventional STM, we acquired STHM images, cf. Figure 3, in order to elucidate the unit cell composition in more detail. To optimize simultaneously the contrast and to exclude possible experimental artifacts, a variety of experimental conditions were also used here. However, determining the stoichiometry from the contrast of the STHM alone (Figures 3c and 1g) is error-prone in this case, since between the molecular rows five bright features per PTCDA molecule are perceived which exceeds the estimated potassium content (see the Methods for details). Furthermore, the contrast of the STM image, showing only one prominent feature in between the molecules, seems to be contradictory to the STHM measurements. In this case, it is indeed indispensable to compare the experimental data to optimized structures and simulated STM images obtained from DFT calculations.

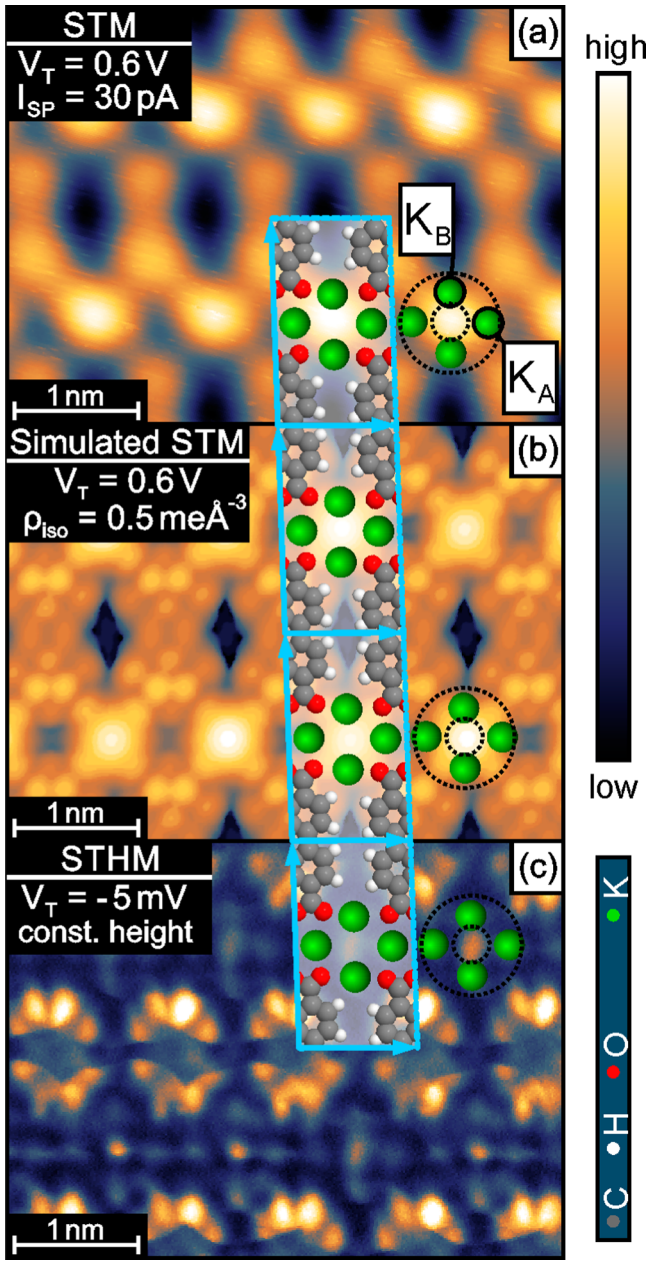

Figure 3. Comparison of experimental STM and STHM images (a, c) with a simulated STM image (b) of the K_4PTCDA phase. The elongated features in STM mode originate from the PTCDA molecules. In the STHM mode, all K atoms are visible as sharp spots, while the bright blurred feature from the simulated and experimental STM (highlighted by the outermost dotted circle) remains visible as a "ghost feature" (highlighted by the innermost dotted circle); see the text for details. The unit cell of the adsorbate layer (blue boxes) comprising the structural model is superimposed in a semitransparent manner. The nonequivalent potassium positions K_A and K_B are marked. Explanations of the displayed quantities are identical to those in Figure 2.

DOI: 10.1021/acsnano.5b07145
ACS Nano 2016, 10, 2365−2374

Therefore, we calculated STM images for a commensurate unit cell as close as possible to the experimentally determined one (see the Methods and the Supporting Information). This unit cell contained 2 PTCDA molecules and 6, 8, and 10 potassium atoms, corresponding to the K_3PTCDA, K_4PTCDA, and K_5PTCDA composites. The optimization of a hypothetical K_3PTCDA results in a structure where some K atoms move underneath the PTCDA, thereby tilting the molecules (see the Supporting Information for structure and simulated STM picture). This clearly contradicts the experimental observation of flat-lying molecules. The structurally optimized configuration with three potassium atoms (see the Supporting Information) does not show the same symmetry as the experimental data. In contrast, for K_4PTCDA the calculated constant current STM picture (Figure 3b) reproduces the experimental data very well (Figure 3a). Even specific details observed in STHM are reproduced in the simulations, such as the inner structure of PTCDA, where the most intense features can be related to C−C bonds near the carboxylic oxygen atoms (as in the case of K_2PTCDA). The most prominent feature localized in between four neighboring PTCDA molecules visible in the experimental STM image has a rather broad and blurred appearance. An almost identical feature at and in between the actual K positions known from the structural optimization (cf. insets in Figure 3) is seen in the STM simulation, which matches the experimental data perfectly. A similar observation, where multiple adatoms are imaged as a single feature in experimental and simulated scanning tunneling topographies, was reported for Cu dimers in the template growth of metal−organic chains on Cu(110).[34]

Considering that the Tersoff−Hamann-based STM simulations originate from a calculation of the density of states between the Fermi level (E_F) and the energy corresponding to the given tip bias, this means that there is a significant unoccupied density of states in the region between the K atoms somewhat above E_F. This density of states can be traced back to a specific state in a suitably charged K_4 cluster, which is characterized by a significant amplitude in the wave function right between the K atoms. Assuming a charge transfer of approximately one electron per K atom to the PTCDA layer and the Ag(111) substrate (see charge transfer analysis in the Supporting Information), it is indeed possible to identify a state with the required properties as the LUMO of a K_4^{4+} cluster. On the surface this state is energetically broadened as a consequence of hybridization with Ag states (a more detailed discussion of the LUMO of a charged K_4 cluster can be found in the Supporting Information).

Comparing the simulated and experimental STM images to the STHM image (Figure 3), notable differences arise for the actual visibility of the K atoms. While the four potassium atoms are individually resolved only in the STHM image, a fifth bright "ghost feature" is simultaneously visible in between the identified K positions, though significantly more narrow and less intense than in the STM measurements and simulations. This is attributed to the fact that for the chosen parameters the contrast obtained by STHM is not purely topographic, but to a certain extent also electronic (as evidenced by the nice agreement of the submolecular contrast between experimental STHM and simulated STM image discussed above). Consequently, the "ghost feature" constitutes a remnant of the intense, blurred feature observed in the genuine STM mode, and we emphasize that without the DFT calculations it is easily mistaken for a fifth K atom.

Considering the energetics of the different stoichiometries also provides insight into the formation of the different phases: In the calculations, we find that for an intermediate K concentration the coexistence of the K_2PTCDA and K_4PTCDA phases is energetically favorable over the formation of a K_3PTCDA phase. In particular, for the presence of an average of three potassium atoms per PTCDA molecule on the surface having half of the surface covered by a K_2PTCDA layer and half by a K_4PTCDA layer is energetically favorable by 0.42 eV per PTCDA molecule over a homogeneous K_3PTCDA coverage. This is in excellent agreement with the above-described experiments. In contrast, at higher K coverages (four potassium atoms per PTCDA molecule), a homogeneous K_4PTCDA layer is by 0.59 eV per molecule more stable than the coexistence of K_3PTCDA and K_5PTCDA domains. All this points toward the particular stability of K_4PTCDA (a table reporting all relevant energies is contained in the Supporting Information). In passing we note that the resulting electronic structures of the intercalated K_2PTCDA and K_4PTCDA phases adsorbed on the Ag(111) substrate are described and compared to pristine PTCDA/Ag(111) briefly in the Supporting Information.

Overall, the structure of the adsorbate can be described by a monomolecular unit cell that contains four potassium atoms per PTCDA, which justifies the above designation of this structure as K_4PTCDA. Compared to the former K_2PTCDA phase, the changed lattice parameters imply an increase of the surface area per molecule of 18.3%, offering the necessary space for the additional K atoms. The corresponding structure exhibits a stripelike assembly of alternating K and PTCDA rows oriented alongside $\vec{a}_1$, similar to the K_2PTCDA phase but with some notable differences: The formerly mentioned relative shift of adjacent rows of PTCDA along $\vec{a}_1$ (by about half of its length) has disappeared now. The molecules are arranged in an essentially rectangular pattern and are almost parallel to the long lattice vector $\vec{a}_2$. The STHM investigations reveal that K again prefers the direct environment of the anhydride groups of PTCDA, similar to the K_2PTCDA phase. However, in the current K_4PTCDA case, not all K atoms attain equivalent positions in the unit cell. In general, two nonequivalent positions of K with respect to PTCDA are observable in STHM: the first (K_A) in between two molecules along $\vec{a}_2$, near carboxylic and anhydride oxygen atoms; and the second (K_B) in between two molecules along $\vec{a}_1$, in the vicinity of carboxylic oxygen atoms only. Interestingly, these positions bear resemblance to the K_2PTCDA case, where the K atoms have a carboxylic and an anhydride oxygen as nearest neighbors in one of the adjacent PTCDA rows, while the nearest neighbor atoms in the other row are only carboxylic oxygens. Furthermore, the DFT analysis shows that again the oxygens of the functional groups of PTCDA in the K_4PTCDA phase tend to bend away from the surface (briefly shown in the Supporting Information), similar to the K_2PTCDA case.

Intriguingly, the experimentally determined epitaxy types of K_2PTCDA and K_4PTCDA are both point-on-line with respect to the Ag(111) substrate, albeit with different registries. This means that the adsorbate unit mesh is an integer multiple of the substrate grid in only one dimension, while in the second dimension no such coincidence of periodicities occurs. In fact commensurate supercells would contain too many molecules to be physically meaningful.[29] Consequently, all constituents of the corresponding adlayers occupy in principle different adsorption sites on the substrate. As a consequence one

DOI: 10.1021/acsnano.5b07145
ACS Nano 2016, 10, 2365−2374

might expect local displacements of the adsorbed entities in order to counterbalance unfavorable substrate sites. On the other hand, even small (sub-Ångström) structural relaxations will usually result in a sizable energy penalty originating from the interactions within the adsorbate layer. While local displacements of adatoms or molecules are not accounted for in our structural analysis of the K_2PTCDA and K_4PTCDA phases, we cannot completely exclude them either. In fact, especially the STHM contrast of the potassium atoms in Figures 1g and 3c suggests that they indeed relax structurally to a certain extent, though our experimental resolution does not allow for a definitive statement here.

Finally, we comment on an interesting feature observed when varying the tunneling voltage in STM mode: As shown in Figure 4 the (blurred) feature associated with all four K atoms

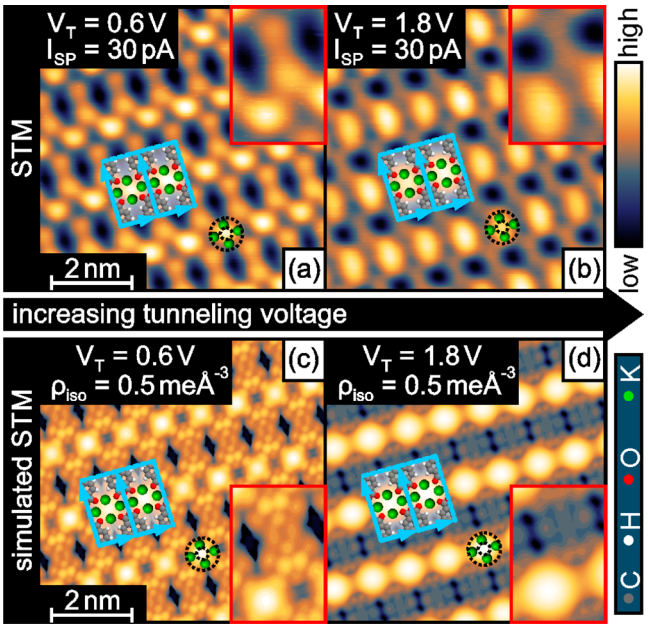

Figure 4. Tunneling-voltage-dependent contrast of the experimental STM images (a, b) compared to the simulated STM images (c, d). Each image comprises a close-up inset for a direct comparison of features associated with PTCDA and K. The unit cell of the adsorbate layer (blue boxes) comprising the structural model is superimposed in a semitransparent manner. Explanations of the displayed quantities are identical to those of Figure 2.

becomes increasingly dominant when raising the tip bias both in experiments as well as in simulations. This similarity between experiments and simulations further supports the suggested assignment of the structural details of the K_4PTCDA layer. In essence, the drastic increase in brightness of the K-induced feature as compared to PTCDA can be related to two effects: First, a larger fraction of the K_4^{4+} LUMO-derived feature in the density of states comes to lie energetically between E_F and the tip bias, when the latter is increased. Additionally, it can be explained by the reduction of the local work function due to the electron transfer from the K atoms to the surface.[35,36] The latter effect is known to influence STM images.[37,38] In our case, the effect is cooperatively enhanced at the center of the K_4 arrangement. Notice that while the increased density of K atoms reduces the individual dipole moments, such a depolarization effect is expected to play only a minor role here, as has been shown for K in dense arrangement on Cu(001).[39] Hence, the electronic states close to the potassium atoms extend more strongly toward vacuum. In contrast, due to the electron accepting character of PTCDA a local increase of the potential barrier can be expected above the molecules. When the voltage is raised from 0.6 to 1.8 V, the tip moves farther from the surface to keep the current constant. Consequently, the relative intensity of electronic states above the potassium is enhanced. Only the detailed shape of the feature stemming from the four K atoms, which becomes slightly elongated in the direction perpendicular to the PTCDA rows in the experiments, is not reproduced in the simulations and is not yet understood.

Further K Intercalation Stages. Exceeding an effective stoichiometry of four potassium atoms per molecule by continuing K evaporation onto the pristine PTCDA/Ag(111) results in another highly ordered $K_{x>4}$PTCDA phase. However, the corresponding self-assembled structure tends to degrade at room temperature within about 1 h (depending on the amount of molecules in the intercalated phase), hampering ST[H]M experiments to determine structure and stoichiometry. Furthermore, the decomposition occurs under reformation of the K_4PTCDA phase, which is, therefore, assigned as the K intercalated PTCDA phase exhibiting the highest potassium content with long-term stability on the Ag(111) surface at room temperature (LEED images showing the structure of the K_4PTCDA phase and its degeneration over time are attached in the Supporting Information).

CONCLUSIONS

By controlled potassium evaporation onto pristine PTCDA monolayer domains on Ag(111) (submonolayer coverage) we observed drastic changes in the molecular arrangement resulting in structural reordering processes of the K intercalated layers. Therefore, new K_xPTCDA phases for x = 2 and 4 could be achieved without the need of any additional annealing steps. By combining complementary experiments (LEED, ST[H]M) and DFT-based modeling, we were able to understand the atomistic details of the formed phases and their stability.

Our data clearly point to a rather strong interaction between K and the PTCDA functional groups: First, the potassium atoms adsorbed in between the molecules initiate the restructuring process of the PTCDA molecules, leading to a complete conversion of the initial system into the K_2PTCDA phase. At higher K concentration, this is then followed by a second transformation into the K_4PTCDA phase. In both cases, (i) K claims similar adsorption positions near the functional groups of PTCDA and (ii) the well-known commensurate registry of the initially pristine PTCDA phase[40] is lifted in favor of point-on-line (POL) coincidences of the K_xPTCDA phases and the Ag(111) substrate.

Our results represent the crucial foundation to assess the electronic structure of such metal-intercalated organic films in greater detail in a consecutive study, since the electronic structure is expected to depend rather sensitively on the mutual alignment between molecules and dopants.

METHODS

All experiments were carried out in an ultrahigh vacuum multichamber system (base pressure in the 10^{-10} mbar region) housing a dual microchannel plate MCP2-LEED from OCI Vacuum Microengineering and an STM purchased from SPECS Surface Nano Analysis GmbH.

DOI: 10.1021/acsnano.5b07145
ACS Nano 2016, 10, 2365−2374

The Ag(111) surface was prepared by multiple cycles of Ar^+ sputtering (700 eV, 2 × 10^{-6} mbar, θ = ± 45°) and annealing (700−800 K). Subsequently, the PTCDA monolayer domains were deposited *via* thermal evaporation at T_{PTCDA} = 560 K (Sigma-Aldrich), purified beforehand by temperature gradient sublimation.[41] The evaporation temperature was stabilized within ΔT = ± 1 K resulting in a constant molecular flux. The evaporation time for a PTCDA submonolayer coverage of 0.7 MLE (monolayer equivalent, referring to a completely filled densely packed monolayer) was determined by combined LEED and STM investigations. To adjust the molar ratio x of potassium atoms with respect to PTCDA molecules (see the Results) of the intercalated phases, K deposition from a commercially available dispenser source (SAES Getters) was realized with a direct current of I = 5.8 A for a given time. Estimations of the relative potassium content difference between different samples are based on the integrated deposition time assuming a constant flux of K atoms. During all deposition experiments the sample was held at room temperature.

Structural investigations were carried out by means of LEED on samples held at room temperature as well as at low temperatures (down to T_{LEED} ≈ 20 K) to ensure that no thermally induced structural changes occur upon cooling. To achieve quantitative LEED measurements the images were corrected regarding distortions of the raw data, by applying a previously published algorithm,[42,43] and subsequently analyzed using the software LEEDLab.[44] All possible rotational and mirror domains were considered, and multiple scattering effects were taken into account during the analysis to further improve the accuracy. For quantitative LEED measurements the lattice parameters of the Ag(111) substrate surface $|\vec{s}_1| = |\vec{s}_2|$ = 2.8894 Å[45] and $\angle(\vec{s}_1,\vec{s}_2)$ = 120° were used as a reference. The relative uncertainties of the absolute values obtained by this procedure are less than 1%.

STM and STHM ($T_{ST[H]M}$ ≈ 1.2 K) were carried out to investigate the unit cell composition in detail. For STHM operation, the chamber housing the STM is exposed to hydrogen *via* a leak valve at p = 1 × 10^{-8} mbar for at least 45 min[22] while scanning the sample with a very low bias voltage and hence at rather small tip−sample distances. Due to the small cross sections of the access windows in the cryogenic shields surrounding the microscope, the precise hydrogen partial pressure in the proximity of the sample is unknown but should be significantly lower than the value given above. Successfully trapping hydrogen in between the tip and the sample surface directly influences the tunneling junction (more details on the STHM contrast are briefly mentioned in the Supporting Information),[22−24,32] resulting in a spontaneous switching in contrast (due to the sensitization of the tip). As this operation mode is unstable for insufficient hydrogen pressure, the latter was adjusted until stable STHM imaging was achieved. Afterward, varying the tunneling parameters (tunneling voltage and current, changing the tip−sample distance) allowed us to tune the resulting convolution of STM and STHM contrast in a given image. Once the tip is sensitized the STHM contrast can be emphasized by lowering the tip−sample distance further (*i.e.*, reducing the tunneling voltage) so as to reach the Pauli repulsive regime. For higher bias voltages when simultaneously moving the tip away from the surface, the STM contrast of the sensitized tip becomes more pronounced and even the trapping of hydrogen can be undone reversibly (allowing to perform STM and STHM with the exactly same tip). Additionally, the imaging is not only very sensitive to the tunneling parameters but also to the tip condition in general (*e.g.*, sharpness and stability). For both STM and STHM measurements, the same KolibriSensor with a tungsten tip from SPECS was used.

In the Results and Discussion we show comparable, but not identical, STHM images obtained under different conditions in order to exclude experimental artifacts. The positions of K and PTCDA within the unit cell were determined for several images so as to avoid possible inconsistencies associated with specific contrasts. This was mainly necessary for the K_4PTCDA phase, but consistency was also checked for the K_2PTCDA phase.

The density functional theory calculations were performed by applying the repeated slab approach using the Vienna ab initio Simulation Package (VASP)[46] in conjunction with GADGET.[47] The Purdew−Burke−Ernzerhof (PBE) functional[48] was applied together with the vdW^{surf} method[49,50] to account for long-range van der Waals interactions. In all calculations, the substrate consisted of five layers of atoms with the bottom three layers fixed during all optimization runs. Off-Γ Monkhorst−Pack[51] k-points grids of 5 × 3 × 1 for K_2PTCDA and 3 × 3 × 1 for K_4PTCDA were used with a Methfessel−Paxton[52] smearing of 0.2 eV. Projector augmented wave (PAW) potentials[53] were used with a cutoff energy of 400 eV for the plane-wave basis set. The STM images were simulated by integrating the local density of states between the Fermi energy (E_F) and the Fermi energy plus the applied tunneling bias (V_T) following the Tersoff−Hamann approach.[31] The integrated density of states (DOS) was then averaged over more than 300 real-space grid points on the surface of a hemispherical tip with a diameter of 2.0 Å.[54] The z-coordinate of the apex of such a model tip, for which the averaged DOS displays a given value (isovalue) was plotted as a function of the lateral position (x,y) as a color map to reproduce the constant current images. A critical assessment of the Tersoff−Hamann approach for the present situation can be found in the Supporting Information.

When the adsorbate is modeled using periodic boundary conditions, a complication arises due to the point-on-line growth of the adsorbate. To overcome this problem, we pursued the following approach: First, the elements of the epitaxy matrices were either rounded to the nearest integer (K_2PTCDA) or first doubled in order to obtain close-to-integer values and then rounded (K_4PTCDA). In the latter case, this would have resulted in a situation with 4 molecules in the unit cell, thereby making the computation tedious. This could be avoided by redefining a supercell being commensurate with the substrate containing only two molecules, as described in the Supporting Information. Next, to ensure intermolecular and K-to-PTCDA distances as in the experiments, while maintaining an epitaxy matrix containing only integer elements, we rescaled the lattice constants of the Ag(111) surface. The necessary (small) changes in the Ag(111) lattice constants and the angles between the substrate unit-cell vectors were different for the systems K_2PTCDA and K_4PTCDA. Different scaling factors along the two unit cell vector directions also had to be applied. The resulting unit-cell dimensions are summarized in the Supporting Information. We verified that these modifications of the lattice have only negligible effects on the electronic properties of Ag. In particular, the work functions of the distorted Ag substrates are practically identical to the work function of the pristine Ag substrate calculated using the optimized PBE lattice constants (see the Supporting Information). Furthermore, the interlayer spacing of the Ag substrate is also comparable.

Layer formation energies were calculated as the differences in total energy of the combined system (K_2PTCDA and K_4PTCDA on the Ag(111) slab) and the total energy of the isolated constituents (*i.e.*, Ag slab, PTCDA molecules, K atoms). The geometries of the combined systems and their constituents were optimized separately.

ASSOCIATED CONTENT

Supporting Information

The Supporting Information is available free of charge on the ACS Publications website at DOI: 10.1021/acsnano.5b07145.

Time-dependent LEED series of the degeneration of K_4PTCDA; STHM series showing the voltage-dependent contrast; possible commensurate K_4PTCDA adsorbate supercells; real space structural models of the optimized structures of K_xPTCDA for x = 2, 3, 4, 5; simulated STM images of K_xPTCDA for x = 3, 5; table of adsorption energies of pristine PTCDA, pristine potassium, and K_xPTCDA for x = 2, 3, 4, 5; lowest unoccupied state of a K_4^{4+} cluster; an analysis of interfacial charge transfer on the basis of Baader charges; a critical assessment of the use of the Tersoff-Hamann approach. (PDF)

DOI: 10.1021/acsnano.5b07145
ACS Nano 2016, 10, 2365−2374

AUTHOR INFORMATION

Corresponding Author

*E-mail: torsten.fritz@uni-jena.de.

Author Contributions

C.Z. and M.G. prepared the samples and performed the LEED and ST[H]M measurements as well as the evaluation of the experimental data. A.B., E.V., and O.T.H. performed the DFT calculations and STM simulations and were assisted by E.Z., G.F., and G.P.B. for interpretation of results. C.Z., M.G., and R.F. prepared the figures and wrote the paper together with A.B., G.F., G.P.B., E.Z., and T.F., who directed the research. All authors jointly discussed the experimental and theoretical results and commented iteratively on the manuscript.

Notes

The authors declare no competing financial interest.

ACKNOWLEDGMENTS

We thank B. Stadtmüller and C. Kumpf for helpful discussions. The computational results presented have been achieved using the clusters of the division for high performance computing at the Graz University of Technology and the Vienna Scientific Cluster (VSC). The work by A.B. was developed within the European doctorate PCAM network. This work was supported by the Deutsche Forschungsgemeinschaft (DFG) through Grant Nos. FR 875/9 and FO 770/2-1 (C.Z., M.G., R.F., T.F.). C.Z. acknowledges funding from the Carl-Zeiss-Stiftung. Financial support by the Austrian Science Fund (FWF) (P24666-N20) is gratefully acknowledged. G.P.B. and G.F. acknowledge support from the MIUR of Italy through PRIN projects DSSCX (No. 20104XET32).

REFERENCES

(1) Walzer, K.; Maennig, B.; Pfeiffer, M.; Leo, K. Highly Efficient Organic Devices Based on Electrically Doped Transport Layers. *Chem. Rev.* **2007**, *107*, 1233−1271.

(2) Reineke, S.; Thomschke, M.; Lüssem, B.; Leo, K. White Organic Light-Emitting Diodes: Status and Perspective. *Rev. Mod. Phys.* **2013**, *85*, 1245−1293.

(3) Iwasaki, K.; Umishita, K.; Sakata, M.; Hino, S. Electrical Conductivity and Electronic Structure of Potassium Doped PTCDA. *Synth. Met.* **2001**, *121*, 1395−1396.

(4) Wuesten, J.; Ziegler, C.; Ertl, T. Electron Transport in Pristine and Alkali Metal Doped Perylene-3,4,9,10-Tetracarboxylicdianhydride (PTCDA) Thin Films. *Phys. Rev. B: Condens. Matter Mater. Phys.* **2006**, *74*, 125205.

(5) Bussolotti, F.; Kera, S.; Ueno, N. Potassium Doping of Single Crystalline Pentacene Thin Film. *Phys. Rev. B: Condens. Matter Mater. Phys.* **2012**, *86*, 155120.

(6) Cheng, C.-P.; Li, T. L.; Kuo, C.-H.; Pi, T.-W. Electronic Structures of Pristine and Potassium-Doped Rubrene Thin Films. *Org. Electron.* **2013**, *14*, 942−950.

(7) Fuentes, G. G.; Knupfer, M. Preparation and Characterization of Single-Phase Potassium-Doped PTCDA Thin Films. *Phys. Rev. B: Condens. Matter Mater. Phys.* **2004**, *70*, 233202.

(8) Wüsten, J.; Berger, S.; Heimer, K.; Lach, S.; Ziegler, C. Interaction of Alkali Metals with Perylene-3,4,9,10-Tetracarboxylic-Dianhydride Thin Films. *J. Appl. Phys.* **2005**, *98*, 013705.

(9) Fuentes, G. G.; Knupfer, M. Electronic Structure and Work Function of Potassium-Doped PTCDA Thin Films. *Appl. Phys. A: Mater. Sci. Process.* **2006**, *84*, 329−333.

(10) Heimer, K.; Wuesten, J.; Lach, S.; Ziegler, C. Interaction of Alkali Metals with Perylene-3,4,9,10-Tetracarboxylic-Dianhydride Thin Films Studied by IR Spectroscopy. *J. Chem. Phys.* **2007**, *126*, 164709.

(11) Wüsten, J.; Heimer, K.; Lach, S.; Ziegler, C. Alkali Metals in Perylene-3,4,9,10-Tetracarboxylicdianhydride Thin Films. *J. Appl. Phys.* **2007**, *102*, 023708.

(12) Zazza, C.; Meloni, S.; Palma, A.; Knupfer, M.; Fuentes, G. G.; Car, R. Quasi-One-Dimensional K−O Chain in PTCDA Thin Films: Evidence from First-Principles Calculations. *Phys. Rev. Lett.* **2007**, *98*, 046401.

(13) Wüsten, J.; Berger, S.; Salomo, M.; Mönnich, A.; Bauer, M.; Lach, S.; Aeschlimann, M.; Ziegler, C. Hot-electron Dynamics in Thin Films of Sodium-Doped Perylene-3,4,9,10-Tetracarboxylic Dianhydride. *Phys. Rev. B: Condens. Matter Mater. Phys.* **2008**, *78*, 195326.

(14) Dienel, T.; Krause, A.; Alle, R.; Forker, R.; Meerholz, K.; Fritz, T. Alkali Metal Doped Organic Molecules on Insulators: Charge Impact on the Optical Properties. *Adv. Mater.* **2010**, *22*, 4064−4070.

(15) Shklover, V.; Schmitt, S.; Umbach, E.; Tautz, F. S.; Eremtchenko, M.; Shostak, Y.; Schaefer, J. A.; Sokolowski, M. Strong K-Induced Changes in Perylene-Tetracarboxylic-Dianhydride Films on Ag(110) Studied by HREELS and LEED. *Surf. Sci.* **2001**, *482*−*485*, 1241−1248.

(16) Hosoi, Y.; Koch, N.; Sakurai, Y.; Ishii, H.; Kampen, T. U.; Salvan, G.; Zahn, D. R. T.; Leising, G.; Ouchi, Y.; Seki, K. Structural Study of Thin Films of Neutral and Potassium-Doped Oligophenylenes on Cu(100). *Surf. Sci.* **2005**, *589*, 19−31.

(17) Tamai, A.; Seitsonen, A. P.; Fasel, R.; Shen, Z.-X.; Osterwalder, J.; Greber, T. Doping-Induced Reorientation of C_{60} Molecules on Ag(111). *Phys. Rev. B: Condens. Matter Mater. Phys.* **2005**, *72*, 085421.

(18) Mercurio, G.; Bauer, O.; Willenbockel, M.; Fiedler, B.; Sueyoshi, T.; Weiss, C.; Temirov, R.; Soubatch, S.; Sokolowski, M.; Tautz, F. S. Tuning and Probing Interfacial Bonding Channels for a Functionalized Organic Molecule by Surface Modification. *Phys. Rev. B: Condens. Matter Mater. Phys.* **2013**, *87*, 121409.

(19) Yang, H.-H.; Chu, Y.-H.; Lu, C.-I.; Yang, T.-H.; Yang, K.-J.; Kaun, C.-C.; Hoffmann, G.; Lin, M.-T. Digitized Charge Transfer Magnitude Determined by Metal-Organic Coordination Number. *ACS Nano* **2013**, *7*, 2814−2819.

(20) Hasegawa, Y.; Yamada, Y.; Sasaki, M. Reordering and Disordering of the Copper Hexadecafluorophthalocyanine (F_{16}CuPc) Monolayer by K Doping. *J. Phys. Chem. C* **2014**, *118*, 24490−24496.

(21) Yano, M.; Endo, M.; Hasegawa, Y.; Okada, R.; Yamada, Y.; Sasaki, M. Well-Ordered Monolayers of Alkali-Doped Coronene and Picene: Molecular Arrangements and Electronic Structures. *J. Chem. Phys.* **2014**, *141*, 034708.

(22) Temirov, R.; Soubatch, S.; Neucheva, O.; Lassise, A. C.; Tautz, F. S. A Novel Method Achieving Ultra-High Geometrical Resolution in Scanning Tunnelling Microscopy. *New J. Phys.* **2008**, *10*, 053012.

(23) Weiss, C.; Wagner, C.; Kleimann, C.; Rohlfing, M.; Tautz, F. S.; Temirov, R. Imaging Pauli Repulsion in Scanning Tunneling Microscopy. *Phys. Rev. Lett.* **2010**, *105*, 086103.

(24) Weiss, C.; Wagner, C.; Temirov, R.; Tautz, F. S. Direct Imaging of Intermolecular Bonds in Scanning Tunneling Microscopy. *J. Am. Chem. Soc.* **2010**, *132*, 11864−11865.

(25) Glöckler, K.; Seidel, C.; Soukopp, A.; Sokolowski, M.; Umbach, E.; Böhringer, M.; Berndt, R.; Schneider, W.-D. Highly Ordered Structures and Submolecular Scanning Tunnelling Microscopy Contrast of PTCDA and DM-PBDCI Monolayers on Ag(111) and Ag(110). *Surf. Sci.* **1998**, *405*, 1−20.

(26) Eremtchenko, M.; Schaefer, J. A.; Tautz, F. S. Understanding and Tuning the Epitaxy of Large Aromatic Adsorbates by Molecular Design. *Nature* **2003**, *425*, 602−605.

(27) Kilian, L.; Umbach, E.; Sokolowski, M. Molecular Beam Epitaxy of Organic Films Investigated by High Resolution Low Energy Electron Diffraction (SPA-LEED): 3,4,9,10-Perylenetetracarboxylica-cid-Dianhydride (PTCDA) on Ag(111). *Surf. Sci.* **2004**, *573*, 359−378.

(28) Rohlfing, M.; Temirov, R.; Tautz, F. S. Adsorption Structure and Scanning Tunneling Data of a Prototype Organic-Inorganic Interface: PTCDA on Ag(111). *Phys. Rev. B: Condens. Matter Mater. Phys.* **2007**, *76*, 115421.

DOI: 10.1021/acsnano.5b07145
ACS Nano 2016, 10, 2365−2374

(29) Hooks, D. E.; Fritz, T.; Ward, M. D. Epitaxy and Molecular Organization on Solid Substrates. *Adv. Mater.* **2001**, *13*, 227−241.
(30) Weller, T. E.; Ellerby, M.; Saxena, S. S.; Smith, R. P.; Skipper, N. T. Superconductivity in the Intercalated Graphite Compounds C_6Yb and C_6Ca. *Nat. Phys.* **2005**, *1*, 39−41.
(31) Tersoff, J.; Hamann, D. R. Theory of the Scanning Tunneling Microscope. *Phys. Rev. B: Condens. Matter Mater. Phys.* **1985**, *31*, 805−813.
(32) Martínez, J. I.; Abad, E.; González, C.; Flores, F.; Ortega, J. Improvement of Scanning Tunneling Microscopy Resolution with H-Sensitized Tips. *Phys. Rev. Lett.* **2012**, *108*, 246102.
(33) Hauschild, A.; Karki, K.; Cowie, B. C. C.; Rohlfing, M.; Tautz, F. S.; Sokolowski, M. Molecular Distortions and Chemical Bonding of a Large π-Conjugated Molecule on a Metal Surface. *Phys. Rev. Lett.* **2005**, *94*, 036106.
(34) Classen, T.; Fratesi, G.; Costantini, G.; Fabris, S.; Stadler, F. L.; Kim, C.; de Gironcoli, S.; Baroni, S.; Kern, K. Templated Growth of Metal-Organic Coordination Chains at Surfaces. *Angew. Chem., Int. Ed.* **2005**, *44*, 6142−6145.
(35) Wandelt, K. The Local Work Function: Concept and Implications. *Appl. Surf. Sci.* **1997**, *111*, 1−10.
(36) Markert, K.; Wandelt, K. The Short Range of the Electronic Promoter Effect of Potassium. *Surf. Sci.* **1985**, *159*, 24−34.
(37) Lang, N. D. Apparent Barrier Height in Scanning Tunneling Microscopy. *Phys. Rev. B: Condens. Matter Mater. Phys.* **1988**, *37*, 10395−10398.
(38) Picone, A.; Fratesi, G.; Brambilla, A.; Sessi, P.; Donati, F.; Achilli, S.; Maini, L.; Trioni, M. I.; Casari, C. S.; Passoni, M.; et al. Atomic Corrugation in Scanning Tunneling Microscopy Images of the Fe(001)-$p(1 \times 1)$O Surface. *Phys. Rev. B: Condens. Matter Mater. Phys.* **2010**, *81*, 115450.
(39) Fratesi, G. Depolarization and Bonding in Quasi-One-Dimensional Na Structures on Cu(001). *Phys. Rev. B: Condens. Matter Mater. Phys.* **2011**, *84*, 155424.
(40) Kraft, A.; Temirov, R.; Henze, S. K. M.; Soubatch, S.; Rohlfing, M.; Tautz, F. S. Lateral Adsorption Geometry and Site-Specific Electronic Structure of a Large Organic Chemisorbate on a Metal Surface. *Phys. Rev. B: Condens. Matter Mater. Phys.* **2006**, *74*, 041402.
(41) Levin, A. A.; Leisegang, T.; Forker, R.; Koch, M.; Meyer, D. C.; Fritz, T. Preparation and Crystallographic Characterization of Crystalline Modifications of 3,4:9,10-Perylenetetracarboxylic Dianhydride at Room Temperature. *Cryst. Res. Technol.* **2010**, *45*, 439−448.
(42) Sojka, F.; Meissner, M.; Zwick, C.; Forker, R.; Fritz, T. Determination and Correction of Distortions and Systematic Errors in Low-Energy Electron Diffraction. *Rev. Sci. Instrum.* **2013**, *84*, 015111.
(43) Sojka, F.; Meissner, M.; Zwick, C.; Forker, R.; Vyshnepolsky, M.; Klein, C.; Horn-von Hoegen, M.; Fritz, T. To Tilt or Not to Tilt: Correction of the Distortion Caused by Inclined Sample Surfaces in Low-Energy Electron Diffraction. *Ultramicroscopy* **2013**, *133*, 35−40.
(44) The software 'LEEDLab' version 1.64 is commercially available from Scienta Omicron at http://www.scientaomicron.com/en/products/350/1155.
(45) Lide, D. R., Ed. *CRC Handbook of Chemistry and Physics*, Internet Version 2005; CRC Press: Boca Raton, 2005.
(46) Kresse, G.; Furthmüller, J. Efficient Iterative Schemes for *ab initio* Total-Energy Calculations Using a Plane-Wave Basis Set. *Phys. Rev. B: Condens. Matter Mater. Phys.* **1996**, *54*, 11169−11186.
(47) Bučko, T.; Hafner, J.; Ángyán, J. G. Geometry Optimization of Periodic Systems Using Internal Coordinates. *J. Chem. Phys.* **2005**, *122*, 124508.
(48) Perdew, J. P.; Burke, K.; Ernzerhof, M. Generalized Gradient Approximation Made Simple. *Phys. Rev. Lett.* **1996**, *77*, 3865−3868.
(49) Ruiz, V. G.; Liu, W.; Zojer, E.; Scheffler, M.; Tkatchenko, A. Density-Functional Theory with Screened van der Waals Interactions for the Modeling of Hybrid Inorganic-Organic Systems. *Phys. Rev. Lett.* **2012**, *108*, 146103.
(50) Tkatchenko, A.; Scheffler, M. Accurate Molecular Van Der Waals Interactions from Ground-State Electron Density and Free-Atom Reference Data. *Phys. Rev. Lett.* **2009**, *102*, 073005.
(51) Monkhorst, H. J.; Pack, J. D. Special Points for Brillouin-Zone Integrations. *Phys. Rev. B: Condens. Matter Mater. Phys.* **1976**, *13*, 5188−5192.
(52) Methfessel, M.; Paxton, A. T. High-Precision Sampling for Brillouin-Zone Integration in Metals. *Phys. Rev. B: Condens. Matter Mater. Phys.* **1989**, *40*, 3616−3621.
(53) Kresse, G.; Joubert, D. From Ultrasoft Pseudopotentials to the Projector Augmented-Wave Method. *Phys. Rev. B: Condens. Matter Mater. Phys.* **1999**, *59*, 1758−1775.
(54) Heimel, G.; Romaner, L.; Brédas, J.-L.; Zojer, E. Organic/Metal Interfaces in Self-Assembled Monolayers of Conjugated Thiols: A First-Principles Benchmark Study. *Surf. Sci.* **2006**, *600*, 4548−4562.

DOI: 10.1021/acsnano.5b07145
ACS Nano 2016, 10, 2365−2374